PAPER NAME

A Combination of Monte-Carlo and Damped Least Square Inversion Method for Determining Radon Source i

AUTHOR

Nandi Haerudin

WORD COUNT

5027 Words

CHARACTER COUNT

25272 Characters

PAGE COUNT

14 Pages

FILE SIZE

1.1MB

SUBMISSION DATE

Mar 20, 2023 10:01 AM GMT+7

REPORT DATE

Mar 20, 2023 10:01 AM GMT+7

7% Overall Similarity

The combined total of all matches, including overlapping sources, for each database.

- 2% Internet database
- 4% Publications database
- Crossref database
- Crossref Posted Content database
- 3% Submitted Works database

Excluded from Similarity Report

- Bibliographic material
- Cited material
- Manually excluded sources
- Manually excluded text blocks

Journal of the Earth and Space Physics, Vol. 46, No. 4, Winter 2021, P. 103-116 (Research)

DOI: 10.22059/jesphys.2020.291763.1007174

A Combination of Monte-Carlo and Damped Least Square Inversion Method for Determining Radon Source in Geothermal Case

Haerudin, N.[1*] and Yogi, I. B. S.[2]

1. Associate Professor, Department of Geophysical Engineering, Faculty of Engineering, University of Lampung, Bandar Lampung, Indonesia

2. Assistant Professor, Department of Geophysical Engineering, Faculty of Engineering, University of Lampung, Bandar Lampung, Indonesia

(Received: 16 Nov 2019, Accepted: 9 June 2020)

Abstract

Radon measurement on the surface can represent the subsurface condition. The measured Radon in geothermal field is caused by the source, which is usually a geothermal reservoir. This study did the inversion process for determining the depth and value of Radon Source. Another fact, non-uniqueness of the solution can produce a result with different model parameter combinations. Hence, it can confuse the interpreter to determine the correct model. Based on this case, we proposed an inversion scheme that can minimize the non-uniqueness effect in the Radon data inversion. The scheme is started by Monte-Carlo inversion and finished by damped least-square. Monte-Carlo inversion, as one of the global optimizations, produce an appropriate starting model for the damped least squares. The damped least square method will finish the scheme fast. In order to be sure with the result, the whole scheme is repeated 19 times. The relative RMS error for the synthetic data is 0.07% to 0.28% to a depth difference of 7% from the synthetic model. With this synthetic data inversion test, the inversion scheme was applied to the real data from the Rajabasa Geothermal field. With this scheme, the section AA' gives an error of 0.51% to 0.88% with a depth of 712 m and section BB' gives an error of 5.79% to 5.27% with a depth of 728 m. This result is coherent with the magnetotelluric data in this area.

Keywords: Damped Least Square; Geothermal; Monte Carlo; Radon; Reservoir.

1. Introduction

Radon is abundant in magmatic rock because they contain Uranium-238 as Radon sources. A Radon is a noble gas that dissolves easily in the geothermal fluid. As magmatic rock and geothermal fluid made contact inside the reservoir, the geothermal fluid will be containing a lot of Radon. Hence, it is assumed that the geothermal reservoir is the Radon source (Balcázar et al., 2010). Radon survey in the geothermal area has been carried out by Haerudin et al. (Haerudin et al., 2013) in Rajabasa Geothermal Field and by Haerudin et al. (Haerudin et al., 2016) in the Way Ratai Geothermal Field.

Moreover, the geothermal fluid consists of Radium, which is the nearest Radon source. Hence, Radon will always be produced in the geothermal fluid while it migrates to the surface. The migration follows a diffusion-convection mechanism (Fleischer et al., 1980; Tanner, 1980; Iakovleva and Ryzhakova, 2003; Iskandar et al., 2005). The diffusion process follows the Flick's Law (Schroeder et al., 1965; Mogro-Campero and Fleischer, 1977), which will reach only several meters (Krister and Lennart, 1982). While the significant process that makes Radon move to the surface follow the Darcy's Law of convection. Because Radon migrates from the reservoir in the geothermal fluid, the existence of fault and fracture under the surface becomes an essential factor for the migration (Figure 1).

Radon inside the reservoir is assumed to have starting concentration value as N. That value will be reduced as it travels and decays then becomes N_t. While the Radon source (N) in the reservoir cannot be measured yet, the Radon value of the surface can be measured by Radon detector. From the Radon on the surface, we can backwardly determine the value of the Radon source (N) by using the inversion method.

*Corresponding author: nandi.haerudin@eng.unila.ac.id

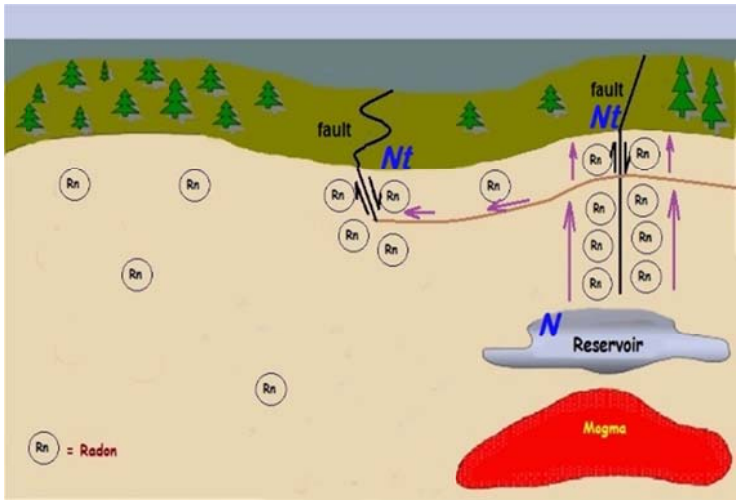

Figure 1. Illustration of Radon migration in the subsurface (modified from (Balcázar et al., 2010)).

2. Forward Modeling

Inversion modeling is applied based on numerical simulation of Radon concentration distribution in the homogenous overburden above an active fault zone (Liu et al., 2008). This simulation is a development of an analytic solution of a simple one-dimensional geometry model (Soonawala and Telford, 2002). This analytic solution was produced based on the Radon movement under the overburden rock, which involves diffusion and convection mechanism. The previous modeling was based on migration simulation of Radon in overburden rock with single fracture and finite width (Abdoh and Pilkington, 1989).

The general formula in this simulation is expressed as:

$$\frac{\partial^2 N}{\partial x^2}+\frac{\partial^2 N}{\partial y^2}-\frac{v_y}{D^*}\frac{\partial N}{\partial y}-\frac{\lambda}{D^*}N=0 \qquad (1)$$

with

λ = Decay constant = 2.1×10^{-6} /s

D^* = Diffusivity = 0.005 cm^2/s

v_y = Convection velocity = 0.008 cm/s

N = Initial Radon concentration (calculated)

According to Equation (1), the numerical solution is created by using the Gauss-Seidel five point stencil of the finite difference method. The boundary condition in this formula follows the von Neumann boundary condition (Figure 2). Besides that, at a depth of y, the Radon value distribution is equal to the Radon Source (N).

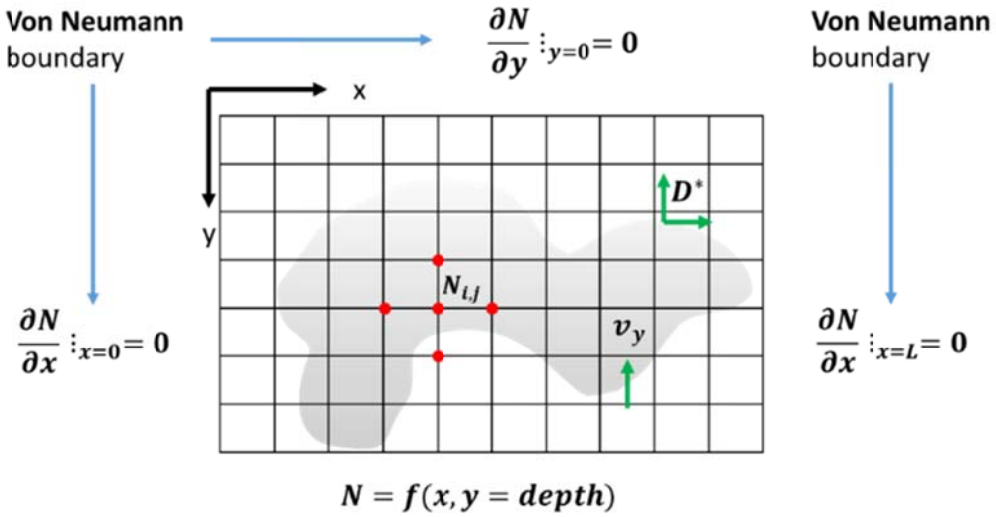

Figure 2. Finite difference calculation for the Radon simulation illustration.

The first derivative formula can be approximated by using finite difference as:

$$\frac{\partial N(x,y)}{\partial x} \approx \frac{N(x+\Delta x,y)-N(x-\Delta x,y)}{2\Delta x} \quad (2)$$

In discrete term, Equation (2) can be written as:

$$\frac{\partial N_{i,j}}{\partial x} \approx \frac{N_{i+1,j}-N_{i-1,j}}{\Delta x} \quad (3)$$

where i is the index for component x and j is the index of component y. Similar to the previous equation, the second derivative of $N(x,y)$ can be approximated by using finite difference as:

$$\frac{\partial^2 N(x,y)}{\partial x^2} \approx \frac{N(x+\Delta x,y)-2N(x,y)+N(x-\Delta x,y)}{\Delta x^2} \quad (4)$$

In discrete term, Equation (4) is written as:

$$\frac{\partial^2 N_{i,j}}{\partial x^2} \approx \frac{N_{i+1,j}-2N_{i,j}+N_{i-1,j}}{\Delta x^2} \quad (5)$$

From both equations above, we can substitute them Equation (1) to become a discrete term

$$N_{i,j} \approx r_y(N_{i+1,j}+N_{i-1,j})+ r_x\left(1-\frac{V_y}{D^*}\right)(N_{i,j+1}+N_{i,j-1})-r_{xy}\frac{\lambda}{D^*}(N_{i,j}) \quad (6)$$

with

$$r_x = \frac{\Delta x^2}{2(\Delta x^2+\Delta y^2)} \quad (7)$$

$$r_y = \frac{\Delta y^2}{2(\Delta x^2+\Delta y^2)} \quad (8)$$

$$r_{xy} = \frac{\Delta x^2 \Delta y^2}{2(\Delta x^2+\Delta y^2)} \quad (9)$$

The calculation process is completed iteratively, so we get a convergent N value distribution, which represents the Radon distribution inside the overburden rock. The Radon value on the surface (Nt) is picked inside the ground with a depth of 70 cm. The Nt value of the simulation is used as data that is compared with the real measured data on the field.

3. Synthetic Model

Following the explanation of forward modeling before, we made a simulation of a synthetic model with 2500 m length and depth of 1000 m. Radon values of the synthetic model is shown in Figure 3a with 10 segments of Radon source. By using that model, we obtained subsurface Radon value distribution (Figure 3b).

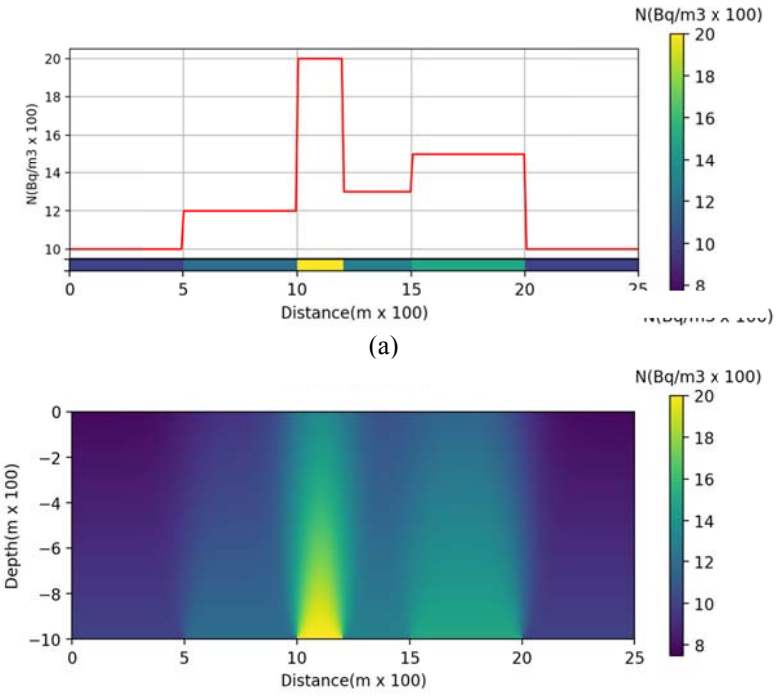

Figure 1. a) Radon source synthetic model at a depth of 1000 m. b) Synthetic Radon distribution in the overburden.

From that data, we selected data with a depth of 70 cm under the surface as synthetic data (Figure 4). From that figure, we can see that the surface value (*Nt*) has a similar pattern with the source (*N*). The synthetic data give two maximum values of the curve, but with a smaller value and narrower than the source. It is happening because of the diffusion and convection of the Radon gas from the source to the surface.

Most of the geophysical methods have a common problem when trying to solve the inverse problem, which is non-uniqueness of the solution (Zhdanov, 2002). A geophysics data can be said inheriting non-unique solution because it can be formed from many combinations of models. In this Radon simulation case, it is known that the simulation of the data can be produced from different models and depth combination. In the example of Figure 5, the model response can be approximated with different depth of 500 m, 1500 m, and 2000 m and the combination of 25 segments of Radon source. This phenomenon can confuse the interpreter, as we chose a bad starting model for the inversion process. Hence, it is necessary to do a step that can give good coarse guidance for choosing the starting model in the inversion process (Maiti et al., 2012).

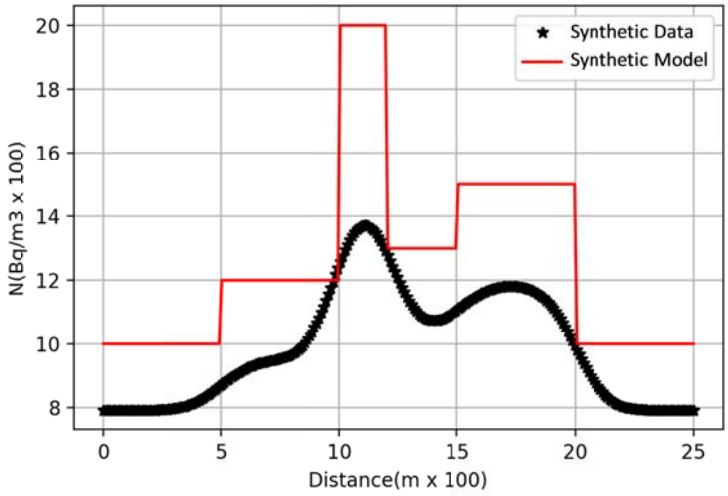

Figure 4. Radon synthetic data at a depth of 70 cm under the surface with a measurement length of 2500 m.

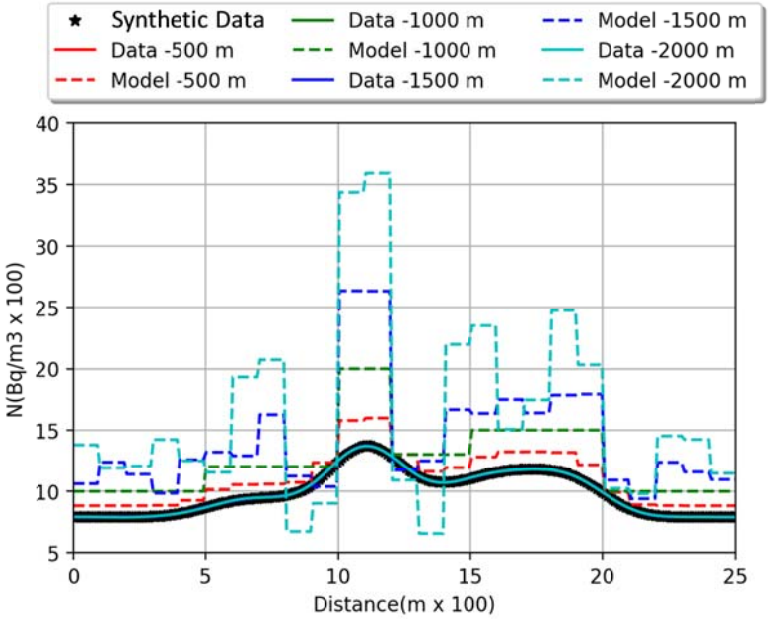

Figure 5. Example of non-uniqueness effect in the Radon data. Different Radon synthetic model combinations can produce similar Radon synthetic data. The models have a depth of 500 m, 1000 m, 1500 m, and 2000 m.

4. Inversion Scheme

The inversion method is usually used for determining the subsurface model or parameter of the measured or observed data. In this Radon method, the measured or observed data is a data measured at a depth of 70 cm under the surface, while the desired model is the Radon distribution and depth of the source in the subsurface. As explained before, the non-uniqueness problem has to be solved first, so that we can be more confident with the inverted model. This problem is widely known to be solved using inversion based on global optimization such as Grid search, Monte-Carlo, Simulated Annealing, Genetic Algorithm and Particle Swarm Optimization (Rubinstein, 1991; Bhattacharya and Sen, 2003; Yogi and Widodo, 2017).

Global optimization requires a lot of long-time computation for obtaining a result with a small error which is similar to the measured data (Chunduru et al., 1997). In this research, the inversion method based on global optimization was used as a guidance for determining the starting model that is expected to reduce the non-uniqueness effect. Therefore, for accelerating the calculation process, the rough model from the global optimization was inverted using the least-square inversion method (Maiti et al., 2012; Yogi and Wido, 2017). More specifically, we used the damped least-square method using the singular value decomposition method.

With that reason, an inversion process that we chose based on the global optimization was the simple method which quickly determines the adequate starting model. The resulted model from this step had an unnecessarily small error, but had a reasonable tendency where the inversion model gathering was good enough. The grid search method is the simplest method, but with more than 10 inversion models, a longer time is required to achieve a final model. The next model that have relatively simple computation is Monte-Carlo method. This method will search the model dimension randomly, so the calculation time was shorter than the Grid search method.

Monte-Carlo method is a random model searching method which gives a model that tends to the minimum global and reduces minimum non-uniqueness effect (Sen and Stoffa, 2013). To get faster model searching, we made a model searching range. We started the model searching range made by averaging the observed data by following the inversion segments. In this case, there were 25 segments with 100 m length. From that average data, the maximum range that was double the average data and the minimum range that was half of the average data were chosen (Figure 6). From the previous simulation, this range meets the characteristic of the diffusion – convection mechanism of Radon. The minimum range was made purposely for accommodating the source segments fluctuation.

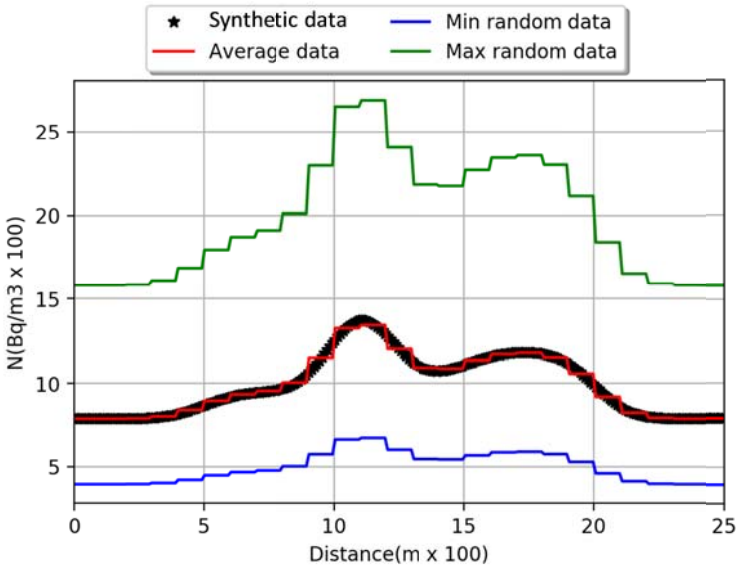

Figure 6. Searching range in the Monte Carlo inversion.

On the other hand, for measuring how good a calculated model is compared to the observed data, we used relative root mean square error (RRMSE) (Jupp and Vozoff, 1975). This relative comparison can give satisfactory result in comparing two different data for every different data range. Given the example, in Figure 7, the first case has a maximum value about 1300 Bq/m^3, while in the second case, the maximum value is about 2700 Bq/m^3. Both cases have a different relative RMS error of 1 %, but the RMS error in the second case (18.7) is greater than the RMS error for the first case (9.4). From that example, we chose RRMSE for measuring two data differences in the later study because of its robustness.

$$\text{Relative RMS error} = \sqrt{\frac{\sum_{i=1}^{N}\left(\frac{d_{obs}-d_{cal}}{d_{obs}}\right)^2}{N}} \quad (10)$$

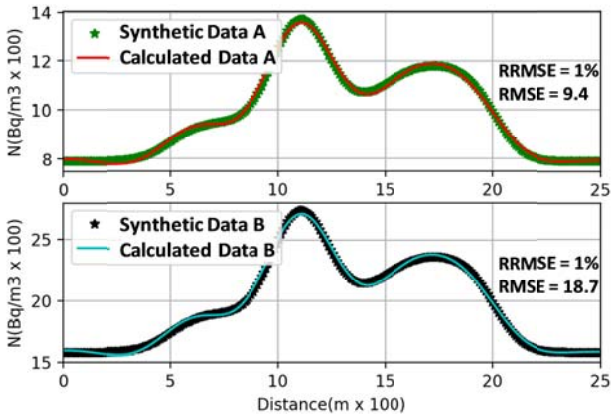

Figure 7. Two responses that have a similar relative root mean square error (RRMSE), but different root mean square (RMS).

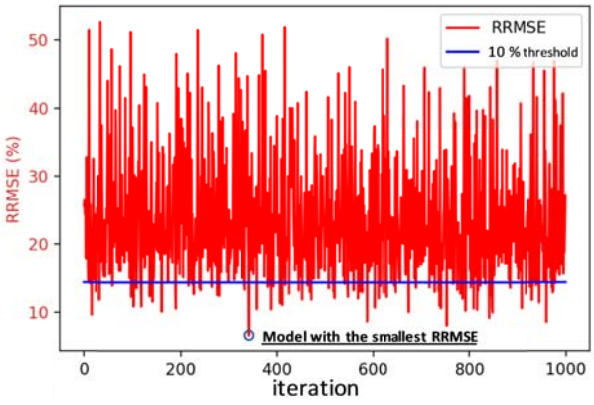

(a)

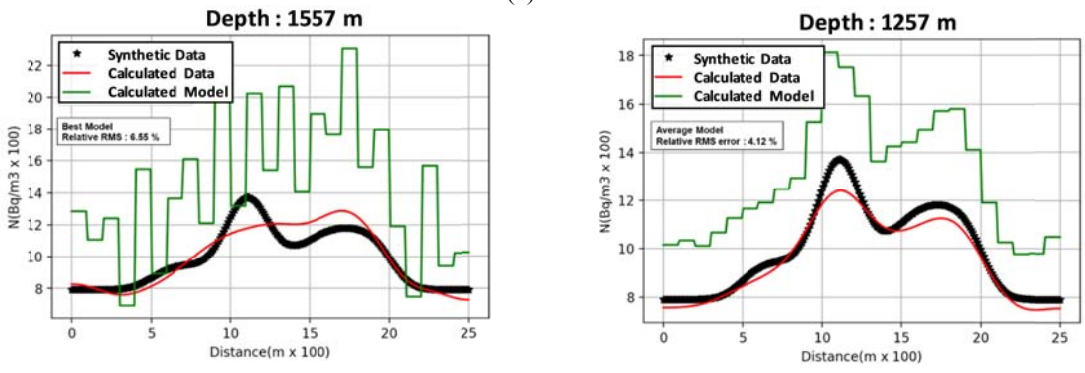

(b) (c)

Figure 8. a) RRMSE value distribution of 1000 iterations from Monte Carlo inversion that shows the smallest error model and the 10% threshold line. b) The smallest error model, and c) average model from the 10% threshold calculated model and calculated data.

From Monte-Carlo calculation, we got 1000 models with the RRMSE range of 6.55% to 52.84% (Figure 8a). In this study, we try to apply two schemes of the final model, which were the best model from the Monte-Carlo calculation and the average model from 10% smallest error model. From these schemes, the first one gave a very fluctuating model, with an error of 6.55% (Figure 8b). The second one gave a model, which had a similar pattern to the data, with an error of 4.12% (Figure 8c). From this result, we chose the model of the second scheme as the starting model for damped least-square inversion (Figure 9).

Forward modeling equation in the previous explanation (Equation 6) can be written in matrix form as Equation (11). **g** represents forward modeling function as in Equation (6), d represents response or calculated data from forward modeling process (Zhdanov, 2002). The response or calculated data here have a similar treatment to the real data, which is picked from 70 cm beneath the surface.

$$\boldsymbol{d} = \boldsymbol{g(m)} \tag{11}$$

where **m** is the model vector, which follows the pattern bellow

$$\boldsymbol{m} = [\mathrm{N}_1, \mathrm{N}_2, ..., \mathrm{N}_n, d] \tag{12}$$

N is the Radon source segment width and d is the depth of the Radon source.

The damped least square algorithm in this study based on singular value decomposition that had been used in (Ekinci and Demirci, 2008) for DC resistivity method. We tried to modify this inversion scheme, suited the Radon method. The damped least square equation is stated as:

$$\Delta \boldsymbol{m} = (\boldsymbol{A}^T \boldsymbol{A} + \varepsilon^2 \boldsymbol{I})^{-1} \boldsymbol{A} \Delta \boldsymbol{d} \tag{13}$$

$\Delta \boldsymbol{m}$ is an update model vector that has m number segments model. $\Delta \boldsymbol{d}$ is a data difference vector between observed data and calculated data from forward modeling process. This vector has n number of elements following the number of the data. $\boldsymbol{A}$ is a Jacobian matrix, $\boldsymbol{I}$ is an identity matrix, and ε is a damping factor. The Jacobian matrix is a matrix of differentiation forward modeling over models which approximated by the forward difference scheme in Equations (14) and (15).

$$\boldsymbol{A} = \frac{\partial \boldsymbol{g}_n}{\partial \boldsymbol{m}_m} \tag{14}$$

$$\boldsymbol{A} = \frac{\boldsymbol{g}_n(\boldsymbol{m}_m + \Delta \boldsymbol{m}_m) - \boldsymbol{g}_n(\boldsymbol{m}_m)}{\Delta \boldsymbol{m}_m} \tag{15}$$

Jacobian matrix, $\boldsymbol{A}$, has a dimension of $n \times m$, where n and m are data number and model parameter number, respectively. The matrix $\boldsymbol{A}$ can be reformed into three different vectors by using singular value decomposition (SVD) method as:

$$\boldsymbol{A} = \boldsymbol{U}\boldsymbol{S}\boldsymbol{V}^T \tag{16}$$

From the singular value decomposition process, the $\boldsymbol{U}$ matrix ($n \times m$) is a data eigenvector, $\boldsymbol{V}$ ($m \times m$) is a model parameter eigenvector. $\boldsymbol{S}$ ($m \times m$) is a diagonal matrix with the value of $\lambda_1, \lambda_2, \ldots, \lambda_m$, this value is also called singular value of $\boldsymbol{A}$ matrix. The correction value of the model parameter in Equation (13) can be expressed again in the new term as:

$$\Delta \boldsymbol{m} = \boldsymbol{V} diag \left\{ \frac{\lambda_j}{\lambda_j^2 + \varepsilon^2} \right\} \boldsymbol{U}^T \Delta \boldsymbol{d} \tag{17}$$

In Equations (13) and (17), we can see that there is a damping factor (ε). This damping factor has a crucial role in regulating the inversion process. The first function is to prevent a matrix singular, which cannot be inverted. The other is to control the convergence speed of the inversion process in Equation (17). We can choose two ways of the damping factor value, which is large or small value. Figure (10) shows the error value that changes every iteration for different choices of the damping factor. When the damping factor is large, the inversion process will be stable because the correction of the model is small. However, it will make the convergence obtained in longer calculation. The other choice is a small damping factor, where the model update is big and the convergence is faster. However, the inversion process cannot be stable.

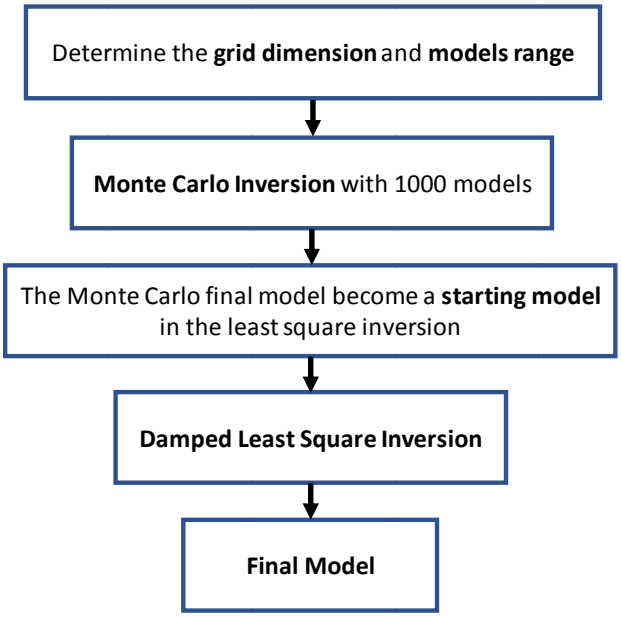

Figure 9. The purposed inversion scheme flow chart.

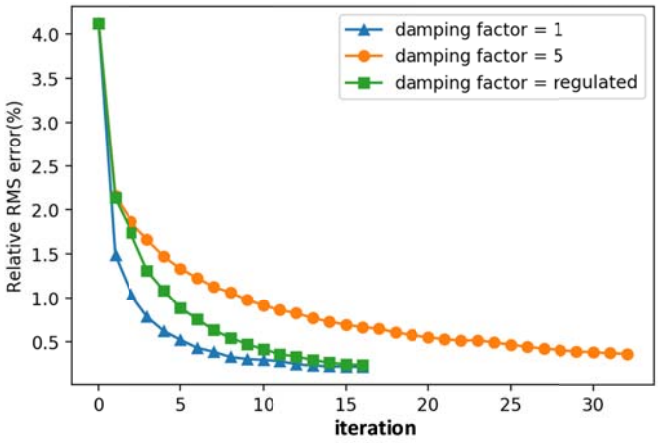

Figure 10. RRMSE curve for every iteration with a different damping factor.

Following that case, the regulation is made for determining the value of the damping factor based on the sensitivity of data over the model. The sensitivity is represented in the Jacobian matrix and λ value at SVD. By using this regulation, at the beginning of the inversion, the damping factor will be large so that the inversion will be stable. Along with the iteration, the damping factor is reduced so that the convergence is faster to be achieved. From this regulation, we can see in Figure 10. The error curve of the regulated damping factor can achieve the same speed with a small damping factor while maintaining the stability. The regulation is shown in equation below (Arnason and Hersir, 1988).

$$\varepsilon = \lambda_L \Delta x^{\frac{1}{L}} \tag{18}$$

where L is trial number for every iteration and Δx is the relative misfit which is calculated with

$$\Delta x_r = \frac{x_{r-1} - x_r}{x_{r-1}} \tag{19}$$

where x_{r-1} is a misfit form the previous iteration and x_r is a misfit from the current iteration.

5. Synthetic Data Inversion

Damped least-square inversion process is started with choosing the staring model. The starting model, in this case, is the final model from Monte-Carlo inversion, which is the average model (Figure 11).

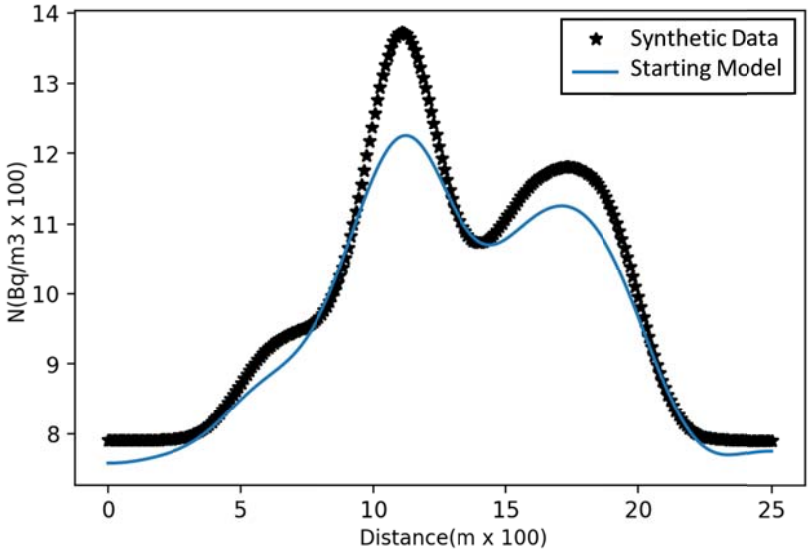

Figure 11. Average model from 10% best model from Monte Carlo that is used as starting model in damped least squares.

Inversion process is finished in some iterations until the error is convergent and one best model achieved. The Figure 12 shows that the calculated curve is approaching the synthetic model. From the quantitative aspect, the error curve will be minimum as the iteration and the calculated response approaching the synthetic data. The inversion stopped when it reached RMS error 0.3% at 16th iteration, where the calculated response gives a similar curve with the synthetic curve.

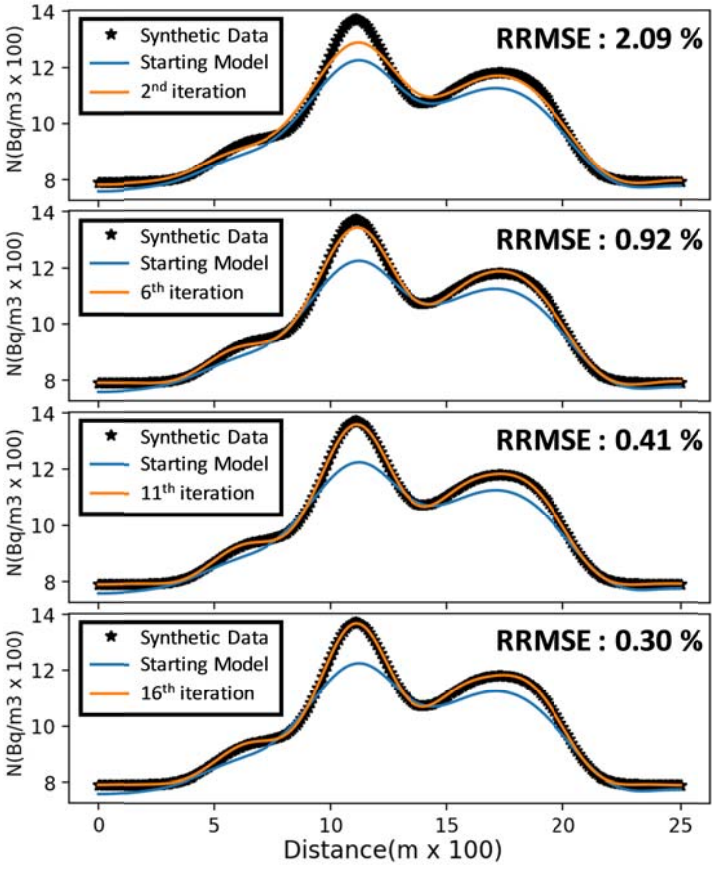

Figure 12. Damped least square processes at 2nd, 6th, 11th, and 16th iteration.

As the inversion model has more segment than the synthetic model, the final model gives us a model that has some difference than the synthetic model. The difference is relatively small as it happened because the model tried to fit the calculated model to the synthetic model. The depth of the model is 1050 m, which is relatively matched by the depth of the synthetic model, 1000 m (Figure 13).

This whole scheme, from determining the starting model to the final model, was repeated for 19 times with the same steps (Figure 14). Therefore, we assumed that all the inversion had a small error, between 0.07% to 0.32%. Besides, the range of the model depth was about 1045 m to 1115 m. From these 19 inversion processes, we know that the average depth of the Radon source is 1070 m. Therefore, we can say that the combination of the Monte-Carlo and Damped least-squares inversion method can overcome and minimize the effect of the non-uniqueness problem.

6. Real Data Inversion

In the previous explanation, we get that the combination of Monte-Carlo and damped least-square inversion successfully inverts the synthetic data. By using that scheme, we tried to solve the real Radon measurement on the field. The measurement was held in Rajabasa geothermal area, Lampung Province in Southern area of Sumatera Island, Indonesia. The Rajabasa geothermal area was located in the area of Rajabasa Mountain (Gunung Rajabasa) (Figure 15). By applying the inversion scheme to the measurement data, we tried to determine the depth of the geothermal reservoir and the value of Radon source. Data from the Rajabasa geothermal area consist of two data sets. The first section is what we call it section AA' with a length about 4000 m. The second section is what we call it section BB', with a length about 3500 m. Both sections were measured directly above the geothermal prospect.

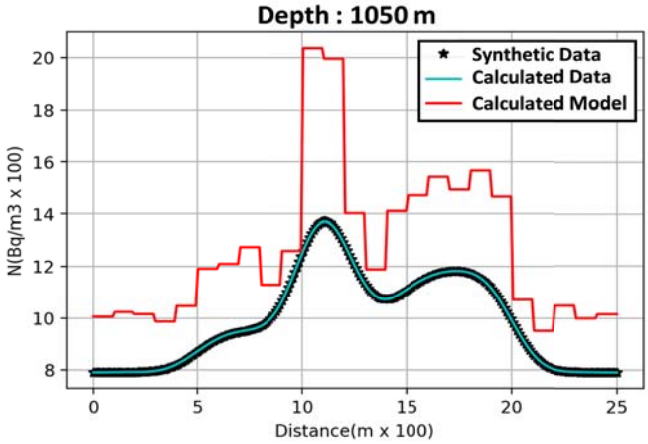

Figure 13. Final model from the synthetic data inversion.

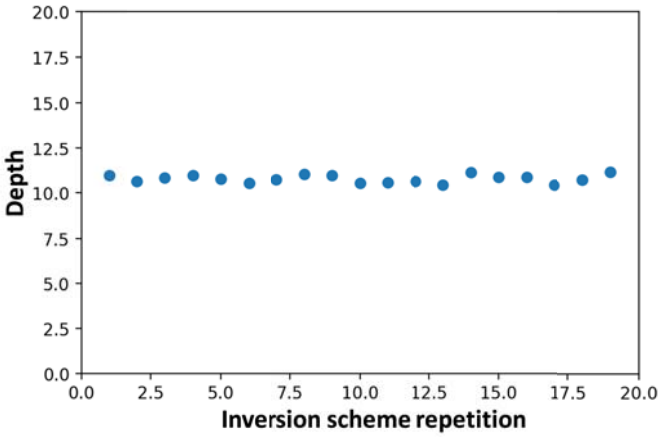

Figure 14. The depth of the inversion scheme results for 19 repetitions that can minimize the non-uniqueness effect.

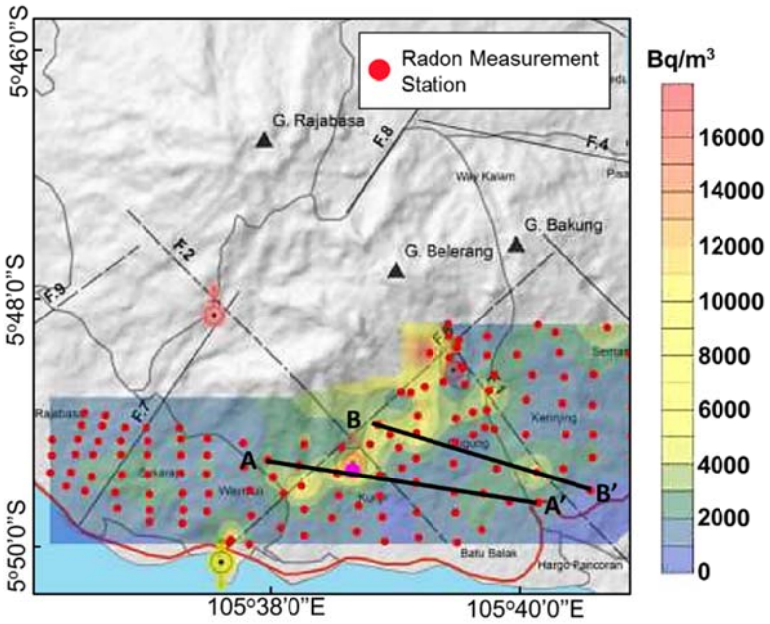

Figure 15. Radon measurement map in Rajabasa Geothermal field.

Section AA' data has three local maximums, which indicate that there are abundant sources underneath the surface (Figure 16a). We applied the inversion scheme to the data with 40 source segments with a width of 100 m. Inversion process was repeated for 19 times. From the repetition, we got the error between 0.51% to 0.88%. The depth range was between 620 m to 797 m, where the average is 712 m (Figure 16b). The final model shows that the Radon source has a maximal value of 8763 Bq/m^3 and the minimum value is 1533 Bq/m^3.

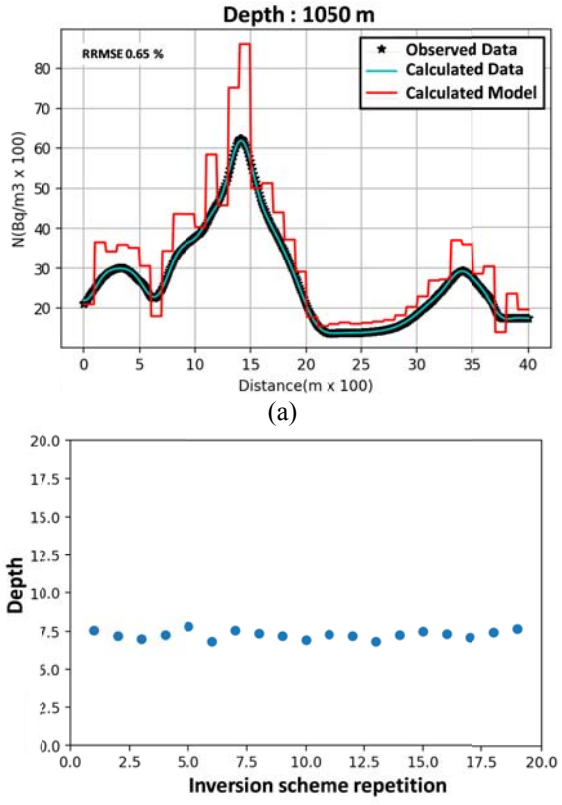

Figure 16. a) Final model from section AA' data inversion. b) Depth of the inversion scheme results for 19 repetitions.

Section BB' was inverted by the inversion scheme with a starting model of 35 segments (Figure 17a). Every segment has a width of 100 m. Similar to the synthetic scheme, the inversion is repeated 19 times. The inversion gives us results that the error was between 5.27% to 5.79%. The depth of the source was a ranged between 682 m to 782 m where the average depth was 728 m (Figure 17b). From the result, we got a bigger relative RMS error than section AA'. It happened because section BB' has fluctuated data. The fluctuation cannot be resolved by using only 100 m. While we can minimize the relative RMS error by reducing the size of the segment, we may get an inappropriate result because of overfitting. When the model segment becomes too small, the inversion process tends to make overfitting final result. We tried to avoid this because the fluctuation might be made from noise. By getting consistent model results is enough, though the relative RMS error was relatively bigger. The result gives a maximum value of 7438 Bq/m^3 and the minimum value of 9 Bq/m^3.

From the two sections above, we know that the depth of source was relatively close, which are 712 m and 728 m. This result confirms the previous result of magnetotelluric measurement by Dimwani et al. (Dimwani et al., 2011). The study showed that the geothermal lied in a depth of 500 m to 1000 m beneath the surface (Figure 18).

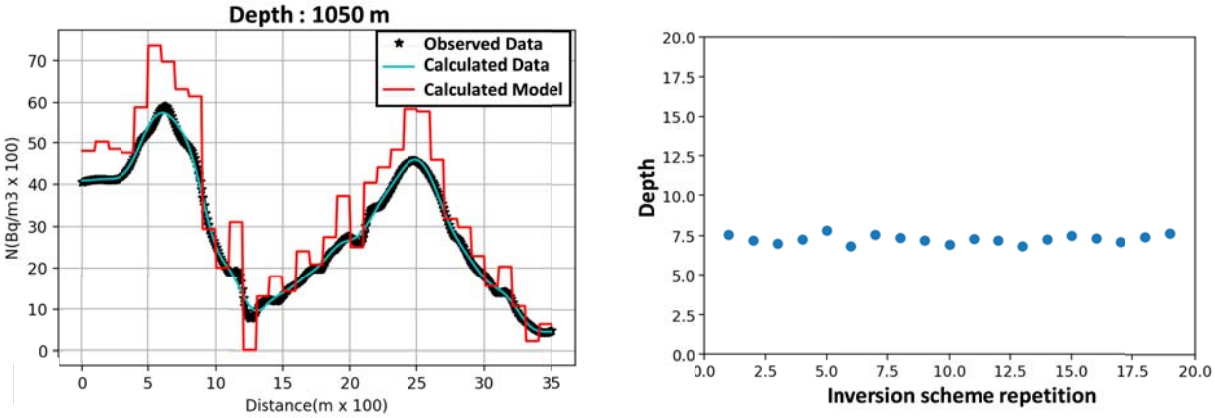

(a) (b)

Figure 17. a) Final model from section BB' data inversion. b) Depth of the inversion scheme results for 19 repetitions.

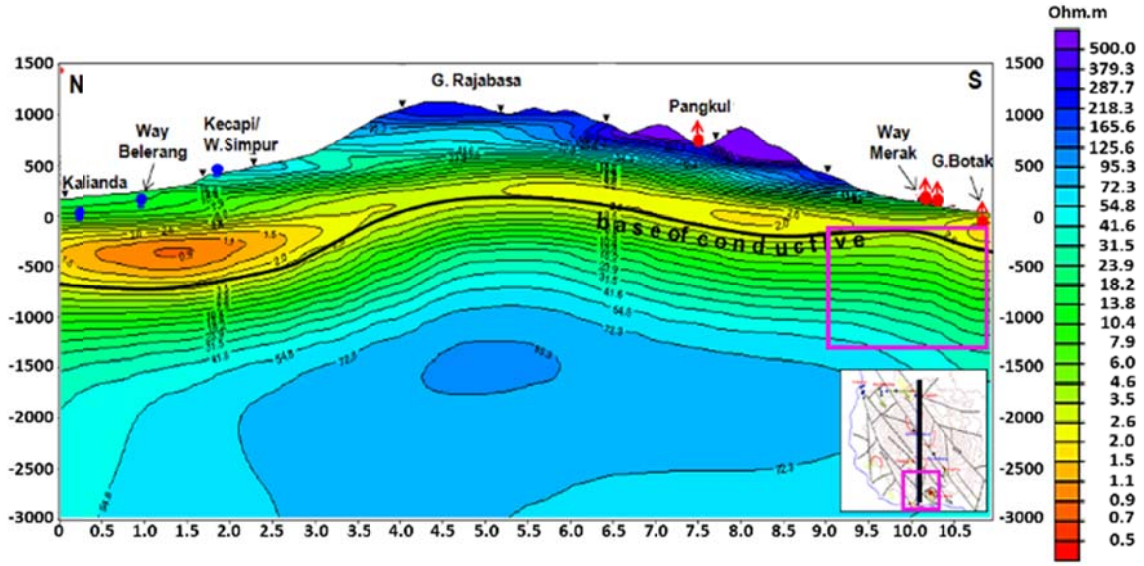

Figure 18. Magnetotelluric section that shows the geothermal reservoir under the conductive layer (Dimwani et al., 2011).

7. Conclusions

Radon measurement on the surface can represent the subsurface condition. From measurement on the surface, we tried to do an inversion. The inversion can show the source parameters, which are the Radon concentration and depth of the source. We proposed a combination of global optimization method and a least square method to overcome non-uniqueness problem while maintaining a fast computation. We used Monte-Carlo and Damped least-square inversion as the Monte-Carlo is a direct and straightforward approach for determining the starting model for the damped least square method. The damped least square variant that we used was based on singular value decomposition. From the experiment, we got that the Monte Carlo process gave adequate starting model to the damped least squares. The damped least squares gave a final model that is similar to the synthetic model, which gave errors between 0.07% to 0.32% in 19 repetitions. From that is repetition, we got a final model that similar to the synthetic model depth. The difference was relatively small, about 7%. We can say that this difference was relatively small because the inversion has considerable uncertainty from the non-uniqueness problem.

From here, we can say that the inversion scheme that we proposed was quite successful. Therefore, we tried to use this scheme to invert the real data. The Radon two sets of data were from Rajabasa geothermal area in Indonesia. There are two sets of data, which are the section AA' and the section BB'. The section AA' inversion gave an error range between 0.51% to 0.88% and the depth of 712 m. On the other hand, from the section BB' we got error in the range between 5.27% to 5.79% with a depth of 728 m. These two final depth results give a consistent result with the magnetotelluric measurement from Dimwani et al. (2011). We can conclude that the inversion scheme of Monte-Carlo and damped least square method can be used for determining the geothermal reservoir depth, especially in Rajabasa geothermal area.

References

Abdoh, A. and Pilkington, M., 1989, Radon Emanation Studies of the Ile Bizard Fault, Montreal, Geoexploration, 25, 341–354.

Arnason, K. and Hersir, G. P., 1988, One Dimensional Inversion Schlumberger Resistivity Soundings, Computer Program, Description and User's Guide,The United Nations University, Geothermal Training, Report 8, 59.

Balcázar, M., Martínez, A. L., Huerta, M., Ruíz, J. F. and Peña, P. 2010, Use of Environmental Radioactive Isotopes in Geothermal Prospecting, 17th Pacific Basin Nuclear Conference.

Bhattacharya, B. B. and Sen, M. K., 2003, Use of VFSA for Resolution, Sensitivity and Uncertainty Analysis in 1D DC Resistivity and IP Inversion, Geophys. Prosp., 51, 393–408.

Chunduru, R. K., Sen, M. K. and Stoffa, P. L. 1997, Hybrid Optimization Methods for Geophysical Inversion, Geophysics, 62, 1196–1207.

Dimwani, W., Pramono, B. Hadi, J. and Alamsyah, O. 2011, Determining Geothermal Concession Area of The Gunung Rajabasa Geothermal Field Based on Magnetotelluric Data, The 11 Th Annual Indonesian Geothermal Association Meeting & Conference, 2011.

Ekinci, Y. L. and Demirci, A., 2008, A Damped Least-Squares Inversion Program for the Interpretation of Schlumberger Sounding Curves, Journal of Applied Sciences, 8, 4070–4078.

Fleischer, R. L., Hart, H. R. and Mogro-Campero, A., 1980, Radon emanation over an ore body, Search for long-distance transport of radon, Nuclear Instruments and Methods, 173, 169–181.

Haerudin, N., Wahyudi, and Suryanto, W., 2013, Radon and thoron analysis of soil gas survey case study of Rajabasa geothermal field, AIP Conference Proceedings, 1554, 218–221.

Haerudin, N., Karyanto, and Kuntoro, Y., 2016, Radon and thoron mapping to delineate the local-fault in the way Ratai geothermal field lampung Indonesia, ARPN Journal of Engineering and Applied Sciences, 11, 4804–4809.

Iakovleva, V. S. and Ryzhakova, N. K., 2003, A method for estimating the convective radon transport velocity in soils, Radiation Measurements, 36, 389–391.

Iskandar, D., Iida, T., Yamazawa, H.,

Moriizumi, J., Koarashi, J., Yamasoto, K., Yamasaki, K., Shimo, M., Tsujimoto, T., Ishikawa, S., Fukuda, M. and Kojima, H. 2005, The transport mechanisms of 222 Rn in soil at Tateishi as an anomaly spot in Japan, Applied Radiation and Isotopes, 63, 401–408.

Jupp, D. L. B. and Vozoff, K. 1975, Stable Iterative Methods for the Inversion of Geophysical Data, Geophysical Journal of the Royal Astronomical Society, 42, 1975.

Krister, K. and Lennart, M., 1982, Evidence for nondiffusive transport of 222Rn in the ground and a new physical model for the transport, Geophysics, 47, 1444–1452.

Liu, J., Wang, Z. and Wang, X., 2008, The numerical simulation and inversion fitting of radon concentration distribution in homogeneous overburden above active fault zones, Applied Geophysics, 5, 238–244.

Maiti, S., Erram, V. C., Gupta, G. and Tiwari, R. K., 2012, ANN based inversion of DC resistivity data for groundwater exploration in hard rock terrain of western Maharashtra (India), Journal of Hydrology, 464–465, 294–308.

Mogro-Campero, A. and Fleischer, R. L., 1977, Subterrestrial fluid convection, A hypothesis for long-distance migration of radon within the earth, Earth and Planetary Science Letters, 34, 321–325.

Rubinstein, R. Y., 1991, Simulation and the Monte Carlo Method, John Wiley and Sons.

Schroeder, G. L., Kraner, H. W. and Evans, R. D., 1965, Diffusion of Radon in Several Naturally Occurring Soil Types, Journal of Geophysical Research, 70, 471–474.

Sen, M. K. and Stoffa, P. L., 2013, Global Optimization Methods in Geophysical Inversion, second., Cambridge University Press.

Soonawala, N. M. and Telford, W. M., 2002, Movement of radon in overburden, Geophysics, 45, 1297–1315.

Tanner, A. B., 1980, Radon Migration in the Ground, A Supplementary Review, in Natural radiation environment III, proceedings of a symposium held at Houston, Texas, April 23-28, 1978, Volume 1 (DOE Symposium Series 51), U.S. Department of Energy, 5–56.

Yogi, I. B. S. and Widodo, 2017, Time domain electromagnetic 1D inversion using genetic algorithm and particle swarm optimization, AIP Conference Proceedings, 1861, 030014-1-030014–14.

Yogi, I. B. S., and Wido, 2017, Implementation of Hybrid Optimization for Time Domain Electromagnetic 1D Inversion, AIP Conference Proceedings, 1861, 030035-1-030035–4.

Zhdanov, M. S., 2002, Geophysical Inverse Theory and Regularization Problems, First., Elsevier Science.

7% Overall Similarity

Top sources found in the following databases:

- 2% Internet database
- Crossref database
- 3% Submitted Works database
- 4% Publications database
- Crossref Posted Content database

TOP SOURCES

The sources with the highest number of matches within the submission. Overlapping sources will not be displayed.

1	School of Business and Management ITB on 2017-03-06 Submitted works	2%
2	coek.info Internet	<1%
3	Ida Bagus Suananda Yogi, Widodo. "Implementation of hybrid optimiz... Crossref	<1%
4	"Potential Theory in Applied Geophysics", Springer Science and Busine... Crossref	<1%
5	A Zaenudin, Rustadi, Iswan, I B S Yogi. "Preliminary study of HVSR for... Crossref	<1%
6	Harmita Lestari, Muhammad Nasri, Andi Zulkifli, Sabrianto Aswad, Sya... Crossref	<1%
7	Qamar, S.. "Adaptive high-resolution schemes for multidimensional po... Crossref	<1%
8	Encyclopedia of Earth Sciences Series, 2011. Crossref	<1%

9	Yunus Levent Ekinci, Alper Demirci. "A Damped Least-Squares Inversio... Crossref	<1%
10	plasma.mephi.ru Internet	<1%
11	Kalscheuer, T.. "Electromagnetic evidence for an ancient avalanche cal... Crossref	<1%
12	Marti@?nez, M.D.. "Inversion of Rayleigh wave phase and group velocit... Crossref	<1%
13	Shengyang Feng, Dongbo Xiong, Guojie Chen, Yu Cui, Puxin Chen. "Con... Crossref	<1%
14	Wahyu Srigutomo, Cahyo Aji Hapsoro, Acep Purqon, Warsa, Doddy Sut... Crossref	<1%
15	link.springer.com Internet	<1%
16	old.vscht.cz Internet	<1%
17	publications.jrc.ec.europa.eu Internet	<1%
18	Praveen Kumar Gupta, Saumen Maiti. "Novel Efficient Method for Auto... Crossref	<1%
19	University of Nottingham on 2021-05-26 Submitted works	<1%

Excluded from Similarity Report

- Bibliographic material
- Cited material
- Manually excluded sources
- Manually excluded text blocks

EXCLUDED SOURCES

jesphys.ut.ac.ir Internet	80%
journals.ut.ac.ir Internet	9%
repository.lppm.unila.ac.id Internet	3%

EXCLUDED TEXT BLOCKS

Department of Geophysical Engineering, Faculty of Engineering, University of Lam...
Yudi Kuntoro, Herru L Setiawan, Teni Wijayanti, Nandi Haerudin. "The Correlation between Radon Emission ...

Department of Geophysical Engineering, Faculty of Engineering, University of Lam...
Yudi Kuntoro, Herru L Setiawan, Teni Wijayanti, Nandi Haerudin. "The Correlation between Radon Emission ...

nandi.haerudin@eng.unila.ac.id
School of Business and Management ITB on 2017-03-06

Journal of the Earth and Space Physics, Vol
arxiv.org

Journal of the Earth and Space Physics, Vol
arxiv.org

Journal of the Earth and Space Physics, Vol
arxiv.org

Journal of the Earth and Space Physics, Vol

arxiv.org

Journal of the Earth and Space Physics, Vol

arxiv.org

Journal of the Earth and Space Physics, Vol

arxiv.org